Title

Incompatibility of standard III-V semiconductor processing techniques with terbium doped InGaAs of high terbium concentration

Journal

Journal of Vacuum Science and Technology A, 30(3)

Authors

Ramu, Ashok
Clinger, Laura
Dongmo, Pernell
et al.

Publication Date

2012-05-31

Incompatibility of standard III–V compound semiconductor processing techniques with terbium-doped InGaAs of high terbium concentration

Ashok T. Ramu[a)]
Department of Electrical and Computer Engineering, University of California, Santa Barbara, Santa Barbara, California 93106

Laura E. Clinger and Pernell B. Dongmo
Department of Materials Science and Engineering, University of Delaware, Newark, Delaware 19716

Jeffrey T. Imamura
Department of Electrical and Computer Engineering, University of California, Santa Barbara, Santa Barbara, California 93106

Joshua M. O. Zide
Department of Materials Science and Engineering, University of Delaware, Newark, Delaware 19716

John E. Bowers
Department of Electrical and Computer Engineering, University of California, Santa Barbara, Santa Barbara, California 93106

(Received 23 December 2011; accepted 23 March 2012; published 16 April 2012)

Terbium-doped InGaAs with a high terbium concentration shows promise as a high-efficiency thermoelectric material, with the thermal conductivity dropping to 1.27 W/m K at a TbAs concentration of 1.55% by number of atoms. However, large discrepancies are noted in Hall effect measurements on terbium-doped InGaAs grown by molecular beam epitaxy on InP substrate following standard III–V wet chemical processing techniques, when compared to samples with no processing beyond deposition of indium contacts. These discrepancies preclude systematic exposition of temperature- and composition-dependent thermoelectric figures of merit. The discrepancy is seen to be correlated with the terbium concentration and the thickness of the active material. The steps in the process sequence are examined under controlled conditions. Although the exact cause for the discrepancy has not been found, some of the obvious reasons have been ruled out. It is therefore surmised that (1) chemical reaction with photoresist, (2) ultraviolet irradiation during photolithography, or (3) reaction with photoresist developing solutions and HF are the factors responsible for the changes in Hall voltage. Evidence is presented for the creation of surface states that corrupt Hall effect measurements on the bulk semiconductor. [http://dx.doi.org/10.1116/1.3701951]

I. INTRODUCTION

III–V compound semiconductors, alloys, and their nanocomposites have gained recognition as having potential for high-efficiency thermoelectric applications. A widely used metric for assessing thermoelectric energy conversion efficiency of a material is $ZT = S^2\sigma T/\kappa$, where S is the Seebeck coefficient, σ is the electrical conductivity, κ is the thermal conductivity, and T is the operating temperature. InGaAlAs doped with erbium has been shown to have thermoelectric properties superior to those of Si-doped InGaAlAs due to simultaneous enhancement of the Seebeck coefficient and thermal resistivity, with ZT increasing to 1.3 at 800 K, compared to 0.6 for Si:InGaAlAs.[1] Recently, III-nitrides, specifically AlInN with very high room-temperature ZT (0.53) have been reported;[2,3] furthermore, the Seebeck coefficient of the optimized material ($Al_{0.83}In_{0.17}N$ with electron concentration $5.1 \times 10^{18}\,cm^{-3}$) shows more than a factor of 2 improvement with modest increase in temperature (82 K), which bodes well for high-temperature applications.[4] InGaN with In ~ 0.3 has shown some promise, with ZT reaching 0.23 at 450 K.[5,6] Seebeck coefficient enhancement has been reported in rare-earth (gadolinium) doped GaN.[7] Doping $Al_{0.14}In_{0.1}Ga_{0.76}N$ with erbium decreases its thermal conductivity from 4 to 1.4 W/m K at room temperature,[8] which is a significant finding in light of the thermal stability of $Al_xIn_{0.1}Ga_{0.9-x}N$ alloy up to 1000 K or more; however ZT of $(Er + Si):Al_{0.1}In_{0.1}Ga_{0.8}N$ remains low, 0.3 at 1055 K. The thermoelectric properties of scandium- and terbium-doped InGaAs have been investigated.[9,10] Of these, Tb:InGaAs stands out because, just as with Er:InGaAs, both the power factor ($S^2\sigma$) and the thermal resistivity increase relative to Si:InGaAs, resulting in a peak ZT (measured) of 0.19 at room temperature. This is to be compared to the simulated value[11] of 0.1 for optimally doped Si:InGaAs.

When the solid solubility of Tb is exceeded in GaAs (Ref. 12) and in InGaAs, TbAs precipitates as nanoparticles. High concentrations of rare-earth elements have been shown[13] to reduce the thermal conductivity of alloys of III–V compound semiconductors below the alloy limit. In Tb-doped $In_{0.53}Ga_{0.47}As$ (hereafter abbreviated to Tb:InGaAs), the thermal conductivity drops to 1.27 W/m K (Ref. 10) at a TbAs

[a)]Electronic mail: ashok.ramu@gmail.com

concentration of 2.47% by number of atoms; this compares very favorably to 4.35 W/m K, the alloy limit for InGaAs, and 4.77 W/m K, the thermal conductivity of InGaAs lattice-matched to InP.[14] All TbAs percentages reported in this work were measured by Rutherford backscattering (RBS) spectroscopy, and InGaAs always refers to the composition lattice-matched to InP, namely $In_{0.53}Ga_{0.47}As$.

The room-temperature *ZT* reaches a peak of 0.19 at 0.8% TbAs in InGaAs, but drops at higher Tb levels, mainly because of the electrical conductivity being strongly impacted by impurity scattering. At higher temperatures two effects may serve to offset this drop of electrical conductivity: (1) the mobility is likely to be limited by lattice scattering rather than impurity scattering, in accordance with general principles of semiconductor transport, thereby becoming comparable to lower doped samples, and (2) the carrier concentration of Tb:InGaAs (0.78% TbAs) increases by ~40% at 600 K compared to its room-temperature value $1.8 \times 10^{18}\,cm^{-3}$, despite degenerate doping. (By contrast, silicon-doped InGaAs showed <10% increase in electron concentration at 600 K compared to its room-temperature value, in spite of a lower doping level, $8 \times 10^{17}\,cm^{-3}$). This unusual donor behavior is likely to become more pronounced at higher TbAs concentrations. The doping regime with >1% TbAs in InGaAs therefore deserves more careful elucidation of its high-temperature thermoelectric figures of merit than is currently available in the literature.

However, it was observed that Hall effect measurements on Tb:InGaAs were severely distorted by standard III–V wet chemical processing, and these distortions were correlated with the concentration of terbium in the alloy and with the film thickness (Table I). This makes Seebeck coefficient measurements on heavily doped samples suspect as well.

In this paper we first outline the typical process sequence used in the fabrication of InGaAs devices. We then present the Hall effect data that led to this investigation. We examine each step in the process, as applied to high-terbium concentration InGaAs, by correlating structure observed using scanning electron microscopy (SEM) with changes in electronic properties observed using Hall effect measurements. We summarize our findings and indicate directions for future work.

II. EXPERIMENTAL SETUP AND METHODOLOGY

All Tb:InGaAs were grown epitaxially on a 500 μm semi-insulating InP substrate using an OSEMI Inc. NextGen® MBE system as described elsewhere.[15] The sample structure consisted of a 100 nm $In_{0.53}Ga_{0.47}As$ buffer layer followed by TbAs codeposited with $In_{0.53}Ga_{0.47}As$. The terbium cell temperature varied from 1189 to 1460 °C. RBS was used to determine, and later calibrate, the percentage of TbAs in InGaAs.[12] The growth rate for $In_{0.53}Ga_{0.47}As$ was ~1 μm/h. The oxide desorption and growth were under As-rich conditions (beam equivalent pressure of As > 10^{-5} Torr); the temperatures for the oxide desorption and growth were 565 and 490 °C, respectively. The growth temperature was monitored by band edge thermometry. Finally, reflective high energy electron diffraction (RHEED) was used to monitor film growth and oxide desorption. During growth, RHEED patterns were very spotty, indicating 3D growth.

The processed samples reported in Table I were fabricated as follows:

(1) Samples were cleaned in acetone/isopropanol/de-ionized water for 2 min each at room temperature, followed by a dehydration bake at 110 °C for 2 min.
(2) Positive lithography using photoresist AZ4210® was used to define mesa, as outlined in Ref. 16, followed by a dehydration bake at 110 °C for 5 min.
(3) Mesas were formed by InGaAs wet etch for 4 min in a 1:1:8 by volume solution of H_3PO_4:H_2O_2:H_2O. This solution etches $In_{0.53}Ga_{0.47}As$ selectively to InP at 400 nm/min.[17] Fluctuations were noted in the etch rate, due to which a 4 min etch was used regardless of film thickness. The large dimensions and correspondingly large tolerances on our device made this overetch feasible.
(4) Photoresist was stripped using acetone, followed by cleaning in isopropanol and de-ionized water, all at room temperature.
(5) The sample surface was encapsulated by plasma enhanced chemical vapor deposition (PECVD) of SiN_x followed by SiO_2 (150 nm SiN_x/300 nm SiO_2). The deposition temperature was 294 °C. This encapsulation layer was intended to arrest any oxidation of the sample during subsequent steps; however, it will be seen later that oxidation is not a concern at temperatures used in this process sequence. Encapsulation remains necessary for high-temperature measurements to prevent sublimation of the sample.
(6) Negative photolithography was done using photoresist AZ5214® as outlined in Ref. 16, followed by a dehydration bake at 110 °C for 15 min.

TABLE I. Hall effect measurements on Tb:InGaAs.

% TbAs	RT conductivity (Ω^{-1} cm^{-1})[a]	RT mobility (cm^2/V s)[a]	RT Hall electron concentration (cm^{-3})[a]	Film thickness (μm)
0.20	402/447/11.2%	4368/4455/2%	5.7×10^{17}/6.3×10^{17}/10.5%	1
0.78	835/940/12.57%	3494/3414/−2.3%	1.5×10^{18}/1.7×10^{18}/13.3%	1
0.99	970/958/−1.2%	3342/2744/−17.9%	1.8×10^{18}/2.2×10^{18}/22.2%	1
1.36	712/805/13.06%	2492/1529/−38.6%	1.8×10^{18}/3.3×10^{18}/45.5%	1
2.47	519/470/−10.4%	1300/916/−29.5%	2.5×10^{18}/3.2×10^{18}/21.9%	1
6.36	131/106/−19.1%	945/452/−52.3%	8.7×10^{17}/1.5×10^{18}/72.4%	0.25
10.89	49/39/−25.6%	1473/187/−87.3%	2.1×10^{17}/1.2×10^{18}/471.4%	0.25

[a]Measurement on as-grown sample with indium contacts/measurement on sample processed as described in Sec. II/deviation in % relative to unprocessed.

(7) The photoresist-coated sample underwent oxygen plasma treatment to remove residual photoresist in the developed areas (100 W, 300 mTorr for 60 s at room temperature).
(8) Buffered hydrofluoric acid (BHF) etch for 9 min etched through PECVD encapsulation layer and exposed the contact areas on the semiconductor surface.
(9) Ti/Au 40 nm/400 nm was deposited by electron beam evaporation.
(10) Excess metal was lifted off in acetone, followed by cleaning in isopropanol and de-ionized water, all at room temperature. *I–V* sweeps showed Ohmic contacts were established without the need for annealing.

Hall effect measurements were performed on as-grown (unprocessed) samples using indium contacts, whose Ohmic behavior was verified for Tb:InGaAs samples. A square van der Pauw[18] geometry was used in all processed samples, with dimensions 4 mm × 4 mm excluding contact pads. The applied magnetic field for all Hall effect measurements was 0.3–0.5 T.

III. RESULTS AND DISCUSSION

Table I summarizes the results of these measurements. The general trend is seen to be that of increasing discrepancy between measurements on as-grown and processed samples as the percent of TbAs increases.

A. Analysis of individual process steps

We now proceed to examine in detail the steps in the sequence of Sec. II. The sample in Table I with TbAs concentration of 10.89% and thickness 0.25 μm was chosen for the studies of this section because it showed the largest distortion in the Hall effect. Oxidation of the thin film due to exposure to atmosphere during storage and transportation was ruled out by the fact that measurements on unprocessed samples were identical over an 8 month period.

The wet-etch solution of step (3) is contraindicated for pure TbAs. Figure 1 shows SEM images of a thin film of pure TbAs (no InGaAs) with a thin capping layer of 50 nm GaAs, before and after a 4 min dip in 1:1:8 H_3PO_4:H_2O_2:H_2O. The sample turned visibly black, and SEM imaging showed drastic changes to the surface morphology, suggesting oxidation of TbAs (GaAs is etched within ~1 min by this solution). Following exposure to the chemical, atomic force microscope (AFM) imaging of the sample showed an rms surface roughness of ~200 nm, proving that the changes to the surface morphology were not restricted to the 50 nm GaAs capping layer.

However, wet etch of 250 nm Tb:InGaAs with 10.89% TbAs in this same solution caused no visible damage to the regions protected by the positive photoresist, except for rough sidewalls (Fig. 2). In particular, it is seen that the surface morphology in the regions protected by the photoresist remains identical before and after wet etch. The dimensions of the sample are 4 mm × 4 mm, so it is unlikely that sidewall roughness was responsible for the observed reduction in

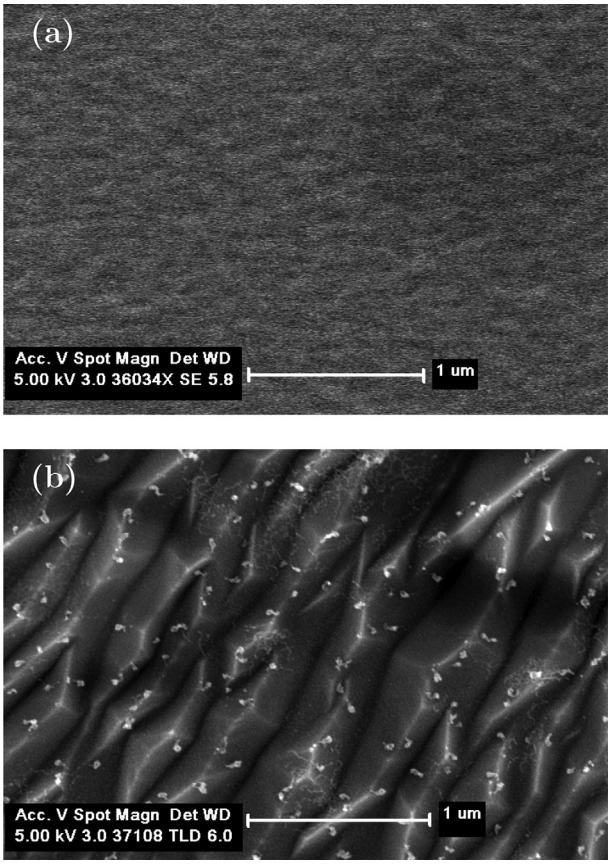

FIG. 1. Plan-view SEM of pure TbAs on InP, with a 50 nm capping layer of GaAs, (a) as-grown and (b) after wet etch of Sec. II, step (3). Magnification ~37 000×, scale bar = 1 μm. Profound changes to surface morphology are seen, presumably due to oxidation of TbAs. The dark area on the upper-right corner of (a) is a charging artifact due to the sample being an insulator.

mobility. Further examination of the mesa under the optical microscope and the SEM showed no evidence of physical damage such as could be attributed to peeling of the resist.

Although SEM imaging gave a negative result, careful exculpation of other steps, as outlined in the remainder of this section, suggests that the chemical reaction of Tb:InGaAs with the constituents of photoresist used for the wet etch was indeed one of the likely sources of discrepancies. We note here that the rough sidewall profile shown in Fig. 2(d) is of interest to the processing of Tb:InGaAs for thermoelectric and optoelectronic applications.

PECVD of silicon nitride [step (5)] was done at 294 °C in a silane/nitrogen/ammonia ambient. RF power was ignited at 22 W after the pressure and flow rates stabilized. The entire film, including active regions and contact pads, was exposed to these conditions at the start of the deposition. Also, in step (8), a 9 min BHF dip is used to etch through the encapsulation layer and expose the semiconductor surface for metallization. Toward the end of this step, Tb:InGaAs is directly exposed to BHF for about 1–2 min. It is essential to investigate PECVD and BHF etch as the possible sources of the discrepancies.

Hence the process was modified as follows. PECVD deposition was eliminated, namely step (5) in. Sec. II. Step (7)

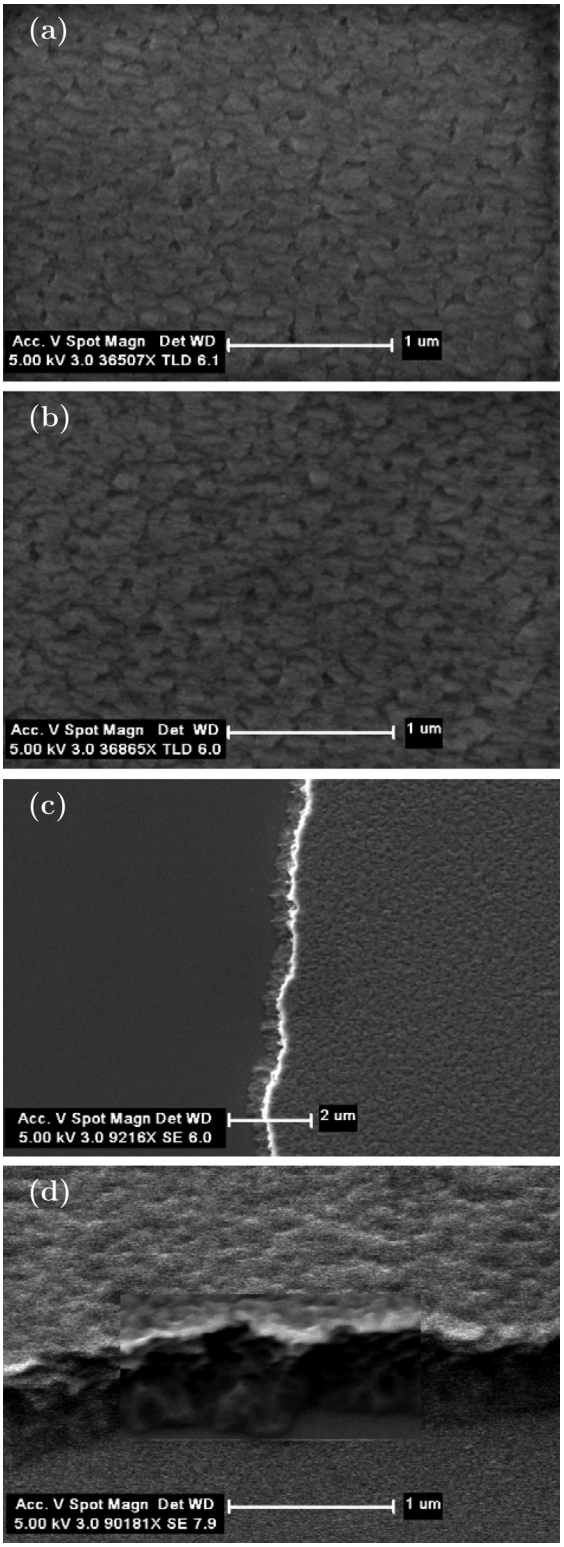

FIG. 2. (a) Plan-view SEM of 10.89% TbAs in InGaAs, before wet etch. Magnification = 36 507×, scale bar = 1 μm. (b) Plan-view SEM of center of mesa etched into 10.89% TbAs in InGaAs, after wet etch of Sec. II, step (3), and photoresist stripping. Under magnification similar to (a), there is no discernible difference in the surface morphology on the mesa before and after etch, as expected. (c) Plan-view SEM of the edge of the mesa after wet etch. Scale bar = 2 μm, magnification = 9216×. (d) Cross-sectional SEM of mesa edge at 90 181× magnification, with a portion of the sidewall shown at higher resolution. This pattern of sidewall roughness is not typical of InGaAs wet etch and is presumably due to oxidation of TbAs. Scale bar = 1 μm.

was also eliminated because it would entail exposing the semiconductor surface directly to oxygen plasma in the contact areas, which would oxidize TbAs. Step (8) was modified to 1:15 HF:H_2O for 30 s, which is necessary to remove native oxide on the contact areas immediately before metallization. All processed samples discussed henceforth underwent this modified process sequence.

With these modifications to the process, the sample with 10.89% TbAs showed a mobility of 488 $cm^2/V\,s$ and a carrier concentration of $4 \times 10^{17}\,cm^{-3}$ after processing, which are quite different from as-grown values (1473 $cm^2/V\,s$ and $2.1 \times 10^{17}\,cm^{-3}$, respectively, see Table I). These discrepancies are, however, much less than those indicated in Table I. A sample of Si:InGaAs (no terbium) was processed in a nearly identical fashion for control purposes; the difference in Hall effect measurements between as-grown ($2.5 \times 10^{18}\,cm^{-3}$, 3374 $cm^2/V\,s$) and processed ($2.3 \times 10^{18}\,cm^{-3}$, 3614 $cm^2/V\,s$) samples was within reasonable bounds.

A final experiment ruled out PECVD unequivocally, and established the 9 min BHF etch as one of the offending steps. The above-described metallized and measured sample was encapsulated by PECVD using the process of step (5). Contact areas were reopened by a 9 min BHF etch and the sample remeasured. Since the sample had already been metallized, BHF made contact only with Au during the etch. The mobility and carrier concentration were now 545 $cm^2/V\,s$ and $3.9 \times 10^{17}\,cm^{-3}$. The small deviations of these values from those measured after metallization but prior to PECVD (488 $cm^2/V\,s$ and $4 \times 10^{17}\,cm^{-3}$) may be attributed to strain from SiN_x/SiO_2 epitaxy and measurement error. Several other samples that did not go through the 9 min BHF etch showed smaller deviations than those that did, despite comparable percent of TbAs and film thickness (see for, e.g., Table II).

The final testable hypothesis was that the sample was degraded by the various heat treatments necessary for photolithography. To rule this out, the thermal conditions during photolithography were simulated by exposing the as-grown sample to 115 °C (the maximum temperature used in any of the photolithography steps) for 30 min in atmosphere. However, no change was observed in the Hall effect measurement following this treatment.

The possible reasons for the residual discrepancies have now been narrowed down to reactions of TbAs with the constituents of photoresists during the mesa etch [steps (2) and (3)], which were perhaps mediated or aggravated by UV exposure during photolithography to define the van der Pauw pattern. Reactions with photoresist developing solutions, and with the diluted HF used to remove native oxide prior to deposition, are also possible reasons, with these reactions affecting only the contact pads. However, as mentioned earlier, *I–V* sweeps confirmed all contacts, indium and Ti/Au, to be Ohmic.

It is to be noted that anisotropy in van der Pauw voltages is present at TbAs concentrations of 4% or more, but this does not explain the large discrepancy in carrier concentrations since the measured Hall coefficient has been shown experimentally and numerically to be insensitive to anisotropy over a large range of values of the anisotropy ratio.[19]

TABLE II. Thickness dependence of process-induced discrepancies in electrical characteristics.

% TbAs	RT conductivity (Ω^{-1} cm^{-1})[a]	RT mobility (cm^2/V s)[a]	RT Hall electron concentration (cm^{-3})[a]	Film thickness (μm)
4.36	184/168/−8.7%	680/668/−1.7%	$1.7 \times 10^{18}/1.6 \times 10^{18}/-5.3\%$	1
3.32	433/429/−0.9%	989/1044/5.6%	$2.7 \times 10^{18}/2.6 \times 10^{18}/-5\%$	0.5
3.32	400/285/−28.8%	901/889/−1%	$2.8 \times 10^{18}/2 \times 10^{18}/-28\%$	0.25

[a]Measurement on as-grown sample with indium contacts/measurement on sample processed using modified sequence of Sec. III A/deviation in % relative to unprocessed.

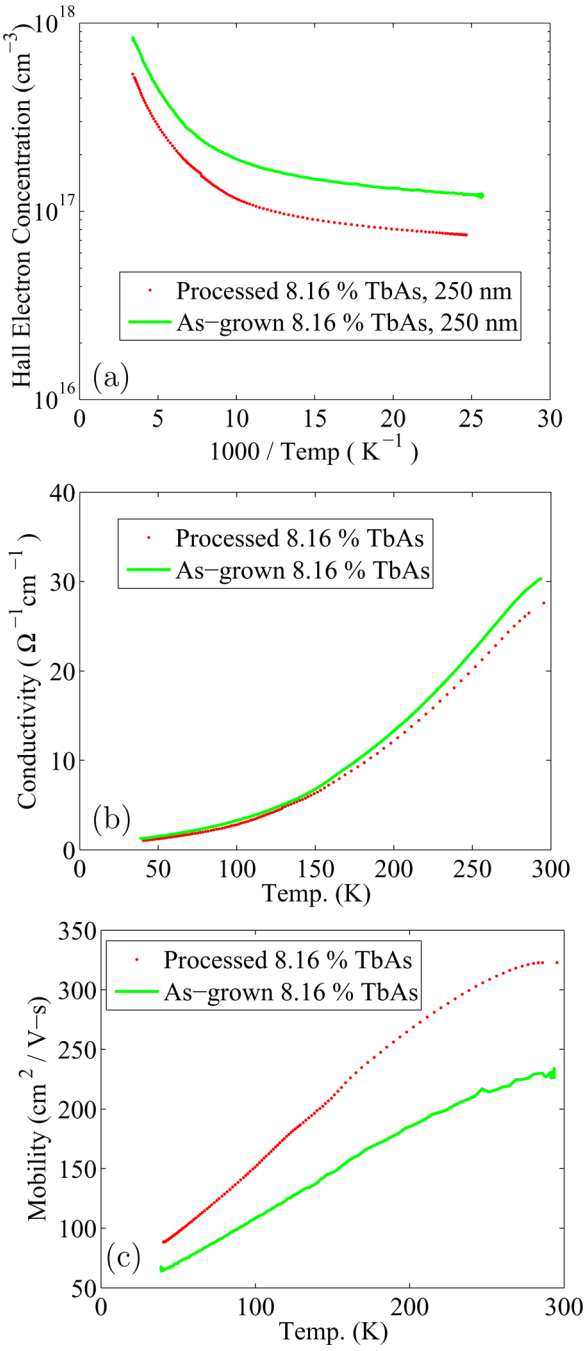

FIG. 3. (Color online) (a) Arrhenius plot of Hall electron concentration in processed and as-grown 250 nm thick 8.16% TbAs in InGaAs. No freeze out of bulk carriers is observed, and processed sample shows lower Hall electron concentration. (b) Plot of electrical conductivity, and (c) plot of Hall mobility as a function of temperature on the same samples. Hall effect data on this material are consistent with the formation of a surface inversion (hole) layer upon processing.

B. Evidence for formation of surface states

We now wish to determine if changes in the material properties due to the process are confined to a surface layer, or if they permeate the entire film. To this end, three samples with comparable TbAs content and carrier concentration, but varying thickness, were processed using the modified sequence of Sec. III A and the Hall effect measurements tabulated (Table II). While the processed 500 nm and 1 μm thick samples showed 10% or less deviation from unprocessed samples, the 250 nm sample showed clear signs of degradation.

This suggests that the standard III–V fabrication process results in the formation of surface states that corrupt Hall effect measurements on thin films. In order to further explore the nature of the surface states, low-temperature Hall effect measurements were conducted on 8.16% TbAs, 250 nm thick Tb:InGaAs. One sample, as-grown except for indium contacts, showed a room-temperature electron concentration of 8.2×10^{17} cm^{-3} and mobility of 231 cm^2/V s. The other sample was processed using the modified sequence of Sec. III A, and showed a room-temperature electron concentration of 5.3×10^{17} cm^{-3} and mobility of 323 cm^2/V s. Figure 3(a) shows an Arrhenius plot of the logarithm of the carrier concentration as a function of inverse temperature. Figures 3(b) and 3(c) show the electrical conductivity and Hall mobility as a function of temperature. The lower electron concentration measured in the processed sample without a proportionate reduction in electrical conductivity is consistent with a surface inversion (*p*-type) layer. However, since the bulk electron concentration did not freeze out even at the lowest temperature used in this study (40 K), we could not determine the areal hole concentration or the mobility of the surface layer. It is also to be noted that the polarity of the surface layer was not consistent from one sample to another; for instance, the 10.89% TbAs sample discussed in Sec. III A showed an increase in Hall carrier concentration after identical processing. Thus no conclusion could be drawn from the available data concerning the nature or distribution of surface states in the bandgap introduced by the processing. However, Table II shows that Hall effect measurements can be made more representative of bulk Tb:InGaAs simply by increasing the film thickness.

IV. SUMMARY AND CONCLUSIONS

Standard III–V compound semiconductor wet chemical processing techniques are incompatible with terbium-doped InGaAs, especially for thin films with high terbium

concentrations (>1% TbAs), as was demonstrated by discrepancies in Hall effect measurements between as-grown and processed samples. BHF etch of the encapsulation layer was proved to be one source of discrepancies. Wherever encapsulation layers are necessary, dry chemical etch techniques must be used to pattern them. The possible reasons for the remaining discrepancies have been narrowed down to reactions with the constituents of photoresists, UV exposure during photolithography, and damage to contact pads due to reaction with photoresist developing solutions and HF. The inverse thickness dependence of the discrepancies suggests the formation of a surface accumulation/inversion layer, as opposed to damage to the bulk of the film.

That InGaAs with high terbium concentration holds promise for high-temperature thermoelectric applications makes it important for this issue to be addressed before reliable data can be reported. Erbium[1] and scandium[9] are similarly used to dope InGaAs in an attempt at improving the thermoelectric figures of merit. Since ErAs is also known to oxidize easily[20] it behooves researchers working on the characterization of transport coefficients of these materials to exercise caution while reporting data on heavily doped samples. Apart from using at least 1 μm thick films as discussed in Sec. III B, shadow-mask evaporation of metal contacts would circumvent photolithography and needs to be considered for such samples, although this would introduce errors due to violation of the requirements of the van der Pauw technique, namely infinitesimally small contacts located on the periphery of the sample.[18]

ACKNOWLEDGMENTS

The authors wish to thank Jonathan Peters, Ajay Raman (Department of Electrical and Computer Engineering, University of California, Santa Barbara), Oliver Bierwagen (Paul Drude Institute, Berlin), Je-Hyeong Bahk (Department of Electrical Engineering, University of California, Santa Cruz), and Ali Shakouri (Electrical Engineering Department, University of California, Santa Cruz) for helpful discussions. A.T.R. and J.T.I. acknowledge support by the Center for Energy Efficient Materials, an Energy Frontier Research Center funded by the US Department of Energy, Office of Basic Energy Sciences, under Award No. DE-SC0001009. This work was funded partially by the DARPA DSO Nanostructured Materials for Power program (US Army, W911NF08-1-0347) and the National Science Foundation through the National Nanotechnology Infrastructure Network.

[1]J. M. O. Zide *et al.*, J. Appl. Phys. **108**, 123702 (2010).
[2]J. Zhang, H. Tong, G. Liu, J. A. Herbsommer, G. S. Huang, and N. Tansu, J. Appl. Phys. **109**, 053706 (2011).
[3]H. Tong, J. Zhang, G. Liu, J. A. Herbsommer, G. S. Huang, and N. Tansu, Appl. Phys. Lett. **97**, 112105 (2010).
[4]J. Zhang, S. Kutlu, G. Liu, and N. Tansu, J. Appl. Phys. **110**, 043710 (2011).
[5]B. N. Pantha, R. Dahal, J. Li, J. Y. Lin, H. X. Jiang, and G. Pomrenke, Appl. Phys. Lett. **92**, 042112 (2008).
[6]B. N. Pantha, R. Dahal, J. Li, J. Y. Lin, H. X. Jiang, and G. Pomrenke, J. Electron. Mater. **38**, 1132 (2009).
[7]E. N. Hurwitz, M. Asghar, A. Melton, B. Kucukgok, L. Su, M. Orocz, M. Jamil, N. Lu, and I. T. Ferguson, J. Electron. Mater. **40**, 513 (2011).
[8]B. N. Pantha, I. Feng, K. Aryal, J. Li, J. Y. Lin, and H. X. Jiang, Appl. Phys. Express **4**, 051001 (2011)
[9]X. Liu, A. T. Ramu, J. E. Bowers, C. J. Palmstrøm, P. G. Burke, H. Lu, and A. C. Gossard, J. Cryst. Growth **316**, 1 (2011).
[10]L. E. Cassels *et al.*, *Electronic Materials Conference*, University of California, Santa Barbara, CA, 22–24 June 2011.
[11]A. T. Ramu, L. E. Cassels, N. H. Hackman, H. Lu, J. M. O. Zide, and J. E. Bowers, J. Appl. Phys. **110**, 083707 (2010).
[12]L. E. Cassels *et al.*, J. Vac. Sci. Technol. B **29**, 03C114 (2011).
[13]W. Kim, J. M. O. Zide, A. C. Gossard, D. Klenov, S. Stemmer, A. Shakouri, and A. Majumdar, Phys. Rev. Lett., **96**, 045901 (2006).
[14]S. Adachi, J. Appl. Phys. **54**, 1844 (1983).
[15]L. E. Clinger, G. Pernot, T. E. Buehl, A. C. Gossard, C. J. Palmstrom, A. Shakouri, and J. M. O. Zide, "Thermoelectric properties of epitaxial TbAs: InGaAs nanocomposites," J. Appl. Phys. (submitted).
[16]See: http://www.nanotech.ucsb.edu/index.php?option=com_content&view=article&id=130:contact-lithography-recipes
[17]A. R. Clawson, Mater. Sci. Eng. **31**, 22 (2001).
[18]L. J. van der Pauw, Philips Tech. Rev. **20**, 220 (1958/59).
[19]O. Bierwagen, R. Pomraenke, S. Eilers, and W. T. Masselink, Phys. Rev. B **70**, 165307 (2004).
[20]U. Singisetti, J. D. Zimmerman, M. A. Wistey, J. Cagnon, B. J. Thibeault, M. J. W. Rodwell, A. C. Gossard, S. Stemmer, and S. R. Bank, Appl. Phys. Lett. **94**, 083505 (2009).